A numerical approach to sound levels in near-surface refractive shadows

Sylvain Cheinet[a)]
French-German Research Institute of Saint-Louis, 5 rue du Général Cassagnou, BP 70034, 68 301 Saint-Louis, France

(Received 6 June 2011; revised 10 January 2012; accepted 13 January 2012)

The present study formulates a consistent method to simulate the outdoor, near-surface sound propagation through realistic refractive conditions. The correlated atmospheric stratification and turbulence properties are derived from standard meteorological quantities through flux-profile similarity relationships. The propagation of a monochromatic sound field is simulated in presence of the turbulence and stratification effects and an impedance ground. The propagation model uses a numerical solution of a second-order moment parabolic equation, which is introduced and evaluated. The so-formed coupled atmospheric-acoustic model is used to systematically investigate the sound levels in near-surface refractive shadows. In an illustrative propagation scenario, the shadow zone sound levels are predicted to show significant variations with the meteorological conditions. Specifically, the sound levels decrease with the adverse wind, as a consequence of enhanced mean upward refraction. Conversely, they increase with the absolute value of the surface heat flux, as a consequence of enhanced turbulence scattering. Implications for the assessment of the sound levels in shadow zones are discussed. © *2012 Acoustical Society of America.*
[DOI: 10.1121/1.3682058]

PACS number(s): 43.28.Gq, 43.28.Fp, 43.28.Js, 43.50.Vt [VEO] Pages: 1946–1958

I. INTRODUCTION

The outdoor sound propagation strongly depends on the atmospheric conditions through the refractive effects. These effects are caused by the spatial fluctuations of the effective sound speed, which depends on the wind, temperature and humidity.

It is customary to distinguish between the mean (ensemble-average) and the remaining (turbulent) contributions in these fluctuations. At moderate to long ranges near the surface, the mean atmospheric stratification may cause a mean upward refraction, resulting in very low sound levels relative to geometrical spreading (hereafter referred to as relative sound levels). The so-called shadow zones appear in the upwind directions, i.e., in typically half the propagation directions from a point source. A mean thermal instability near the surface, as often found in day-time over land, is also favorable to refractive shadowing. Hence, refractive shadows are extremely frequent in outdoor sound propagation considerations. They affect the sound level statistics for any propagation scenario with changing wind directions.

Small-scale atmospheric fluctuations also induce some refractive effects, often referred to as turbulence scattering. Scattering causes the penetration of sound into shadow zones (Daigle *et al.*, 1986). Turbulence is always present in the lower atmosphere. As a result, experimental studies suggest that, at propagation ranges of the order of one kilometer, the relative sound levels do not fall below -30 dB in refractive shadow zones (Wiener and Keast, 1959; Parkin and Scholes, 1964, 1965). Turbulence may also alter the coherence of the signal (Havelock *et al.*, 1995), and reduce the near-surface negative interferences (e.g., Daigle, 1979; Wasier, 1999).

The atmospheric stratification is driven by the meteorological conditions at scales typically greater than 10 km. Weather measurement and prediction systems can document this stratification. They can be coupled to sound propagation models in order to document and predict the sound levels, e.g., Heimann and Gross (1999), Lihoreau *et al.* (2006), Wunderli and Rotach (2011).

In comparison, there are some major research challenges in accounting for the effects of refractive turbulence. First, these effects depend on the turbulence characteristics, which must therefore be documented (Wilson, 2000; Cotté and Blanc-Benon, 2007). Turbulent fluctuations are accounted for only in a parametric manner in weather prediction systems (e.g., Cheinet, 2003). Models of the turbulence characteristics relevant to sound scattering can be developed in terms of predictable meteorological forcings (Wilson, 2000). These models still restrict to near-surface atmospheric levels, and require some assumptions at the edge of current understanding on the structure of atmospheric turbulence (see below).

Second, the description of the impact of turbulence on sound propagation is also an on-going research area. Accounting for this impact has been the subject of many studies (West *et al.*, 1989; Forssén, 2003). Without mean refraction, solutions exist based on the analytical formalism of line-of-sight propagation (Tatarski, 1961; Clifford and Lataitis, 1983). In the presence of refraction, many attempts have used the Parabolic Equation (PE) approach, for the deterministic pressure field (Gilbert *et al.*, 1990; Chevret *et al.*, 1996), and more recently for the second-order statistical moment of the pressure field (Wilson and Ostashev, 2001; Wilson *et al.*, 2009).

[a)]Author to whom correspondence should be addressed. Electronic mail: sylvain.cheinet@isl.eu

These challenges have hampered a systematic, quantitative understanding of the sound characteristics in the shadow zones. Standard procedures for outdoor sound propagation measurements restrict to downwind regions, i.e., outside the shadow zones (e.g., ANSI S12.18, 1994). On the modeling side, a common practice is to calculate the sound levels without turbulence, and set a minimum relative sound level. Heimann and Salomons (2004) use a threshold of -25 dB; Salomons and Heimann (2004) and Defrance *et al*. (2007) use -15 dB. The arbitrariness in this selection reflects that there is a low degree of consensus on the existence of a minimum relative level in terms of the meteorological forcings (e.g., Wiener and Keast, 1959, Fig. 2). In fact, the accuracy and physical basis for this approach remain to be quantified in the general case.

The present study is an effort in that direction. It formulates a consistent method to integrate some state-of-the-art models of the near-surface atmospheric stratification and turbulence and of the sound propagation. This integration allows an original analysis of the sound propagation under arbitrary meteorological forcings. In particular, it is used here to systematically assess the sound levels in refractive shadow zones. The paper is composed as follows. Section II introduces and evaluates the numerical model used to simulate sound propagation in the presence of atmospheric stratification and turbulence. Section III describes the approach to consistently parameterize the relevant mean stratification and turbulent characteristics. Section IV discusses the combined effects of mean refraction and turbulent scattering on the sound level predictions in the near-surface shadow zones. Section V summarizes the results.

II. SOUND PROPAGATION MODEL

A. Description

Let u, T and c denote the atmospheric wind modulus, temperature and sound speed. Consider a two-dimensional (2D) slab of the atmosphere, with z and x the height and horizontal distance (hereafter referred to as range), and θ the angle between the wind and the slab directions. Let the subscript 0 denote a reference value. Let $c_{mov} = c + u\cos\theta$ be the effective sound speed, and ε_{mov} be twice the refractive index fluctuation ($\varepsilon_{mov} = c_0^2/c_{mov}^2 - 1$). A first-order approximation gives [Ostashev, 1994, Eq. (4) and (41)]:

$$\varepsilon_{mov}(x,z,\vec{m}) = -\frac{T(x,z,\vec{m}) - T_0}{T_0} - 2\frac{u(x,z,\vec{m})\cos\theta}{c_0}. \quad (1)$$

The vector $\vec{m}$ holds the dependence on the meteorological conditions. The motivation for the omission of humidity contributions in Eq. (1) is given in Appendix A.

Let p denote the propagating pressure field for a given 2D distribution of ε_{mov}. Let k denote the wave-number of the selected monochromatic signal. Let $g(x,z_1,z_2,\vec{m})$ denote the second-order statistical moment $\langle p(x,z_1,\vec{m})p^*(x,z_2,\vec{m})\rangle$, where $\langle\,\rangle$ is an ensemble average. The average sound level (in dB) at (x,z_1) is ten times the decimal logarithm of $g(x,z_1,z_1,\vec{m})$. Wilson and Ostashev (2001) derive the propagation equation:

$$\frac{\partial g(x,z_1,z_2,\vec{m})}{\partial x} = \Big\{(E(z_1,\vec{m}) + E^*(z_2,\vec{m})) - \frac{k_0^2}{8}q_\varepsilon(x,z_1,z_2,\vec{m})\Big\}g(x,z_1,z_2,\vec{m}). \quad (2)$$

The derivation of Eq. (2) by Wilson and Ostashev (2001) uses a narrow-angle parabolic equation (PE) for the pressure field as starting point. The underlying high-frequency approximation is examined in Sec. III. Sound absorption by air is neglected, which is justified at the ranges and frequencies used in this study (2000 m and 100 Hz). The impact of the transverse wind is neglected [e.g., Ostashev, 1997, Eq. (2.87)]. Finally, their derivation uses the Markov approximation and assumes Gaussian statistics for ε_{mov}.

In Eq. (2), the operator $E(z,\vec{m}) = \frac{i}{2k_0}\frac{\partial^2}{\partial z^2} + \frac{ik_0}{2}\langle\varepsilon_{mov}\rangle(z,\vec{m})$ holds the impacts of diffraction and mean refraction. It does not depend on range by virtue of the ensemble averaging of ε_{mov}. The impact of turbulence in Eq. (2) is held through:

$$q_\varepsilon(x,z_1,z_2,\vec{m}) = b_\varepsilon(x,z_1,z_1,\vec{m}) + b_\varepsilon(x,z_2,z_2,\vec{m}) - 2b_\varepsilon(x,z_1,z_2,\vec{m}). \quad (3)$$

Here $b_\varepsilon(x,z_1,z_2,\vec{m})$ is the projected correlation function of ε_{mov} at (z_1,z_2), it is formally defined in Appendix B. The projection refers to a spatial integration along the x axis [Eq. (B1)]. Whereas b_ε nominally depends on range, the present model does not describe this dependence, which is omitted hereafter.

Let bold characters denote the matrix form of operators and variables with a vertical discretization of the 2D medium in N levels. The $N\times N$ matrixes $\boldsymbol{g}(x,\vec{m})$, $E(\vec{m})$, and $K(x,\vec{m})$ stand for $g(x,z_1,z_2,\vec{m})$, $E(z,\vec{m})$ and $k_0^2\Delta x q_\varepsilon(z_1,z_2,\vec{m})/16$. From Eq. (2), the centered, finite differences equation advancing $\boldsymbol{g}$ over a range step Δx is

$$\boldsymbol{g}(x+\Delta x,\vec{m}) - \boldsymbol{g}(x,\vec{m}) = F(\vec{m})\tilde{\boldsymbol{g}}(x,\vec{m}) + \tilde{\boldsymbol{g}}(x,\vec{m})F^{*T}(\vec{m}) - K(\vec{m})\circ\tilde{\boldsymbol{g}}(x,\vec{m}), \quad (4)$$

where $\tilde{\boldsymbol{g}}(x,\vec{m}) = \boldsymbol{g}(x+\Delta x,\vec{m}) + \boldsymbol{g}(x,\vec{m})$, $\circ$ is the term-by-term (Hadamard) product and $F = E\Delta x/2$. The height resolution is typically chosen as $\Delta z \approx k_0^{-1}$ in PE models. The choice of Δx relates to the numerical solution of Eq. (4), as now discussed.

The phase term of p nominally writes as $\exp(ikx\cos\alpha + ikz\sin\alpha)$ with $k \propto k_0$, and α the angle (of maximum α_m) between the wave vector and the x axis. The amplitude of p fluctuates with l_{tot}, the characteristic size of medium inhomogeneities. Therefore, one obtains $\frac{1}{k_0}\frac{\partial p}{\partial z} \propto \max(\sin\alpha_m, \frac{1}{k_0 l_{tot}})p$ (Ostashev, 1997, p. 50), and

$$Fg \propto k_0\Delta x\frac{1}{4}\max\left(\sin^2\alpha_m, \left(\frac{1}{k_0 l_{tot}}\right)^2, \langle\varepsilon_{mov}\rangle\right)g. \quad (5)$$

One has $\varepsilon_{mov} \ll 1$ in the atmosphere and $(k_0 l_{tot})^{-1} \ll 1$ (Sec. III). Still, in nominal geometries, Eq. (5) gives $Fg \propto k_0\Delta x g$. Wilson *et al*. (2009, p. 373) thus obtain that $Fg \ll g$ only if $\Delta x \ll k_0^{-1} \approx \Delta z$. However, one has

$\sin^2\alpha_m \ll 1$ in the narrow-angle approximation, so Eq. (5) gives $Fg \ll k_0\Delta xg$. Hence, one has $Fg \ll g$ provided that $\Delta x \leq k_0^{-1}$. This result is far less restrictive than the result by Wilson *et al*. (2009). Comparably, from $q_\varepsilon = O(10^{-2})m$ (see Fig. 5 below), one has $k_0^2\Delta xq_\varepsilon/8 \ll k_0\Delta x$ at audible frequencies or below, so $gk_0^2\Delta xq_\varepsilon/8 \ll g$ provided that $\Delta x \leq k_0^{-1}$.

Let $\boldsymbol{Q}(\vec{m})$ denote the matrix of terms $\exp\{-k_0^2\Delta xq_\varepsilon(z_1,z_2,\vec{m})/8\}$. Let $\boldsymbol{R} = \boldsymbol{H}^{-1}\boldsymbol{H}^*$, with $\boldsymbol{H} = \boldsymbol{I} - \boldsymbol{F}$ and $\boldsymbol{I}$ the identity matrix. The equation

$$\boldsymbol{g}(x+\Delta x,\vec{m}) = \boldsymbol{R}(\vec{m})(\boldsymbol{Q}(\vec{m})\circ\boldsymbol{g}(x,\vec{m}))\boldsymbol{R}(\vec{m})^{*T}, \quad (6)$$

is rigorously equivalent to

$$\begin{aligned}\boldsymbol{g}(x+\Delta x,\vec{m}) &- \boldsymbol{Q}(\vec{m})\circ\boldsymbol{g}(x,\vec{m}) + F(\vec{m})(\boldsymbol{g}(x+\Delta x,\vec{m})\\ &- \boldsymbol{Q}(\vec{m})\circ\boldsymbol{g}(x,\vec{m}))F^{*T}(\vec{m})\\ &= \boldsymbol{F}(\vec{m})(\boldsymbol{g}(x+\Delta x,\vec{m}) + \boldsymbol{Q}(\vec{m})\circ\boldsymbol{g}(x,\vec{m}))\\ &\quad + (\boldsymbol{g}(x+\Delta x,\vec{m}) + \boldsymbol{Q}(\vec{m})\circ\boldsymbol{g}(x,\vec{m}))F^{*T}(\vec{m}). \quad (7)\end{aligned}$$

Let Δx be chosen as a fraction of the acoustic wavelength: $k_0\Delta x < 1$. From the above paragraph, Eq. (7) can be approximated as follows. First, the third left-hand side term is neglected. Second, one may use $\boldsymbol{Q}(\vec{m})\circ\boldsymbol{g}(x,\vec{m}) \approx \boldsymbol{g}(x,\vec{m})$ in the right-hand side terms. Third, $\boldsymbol{Q}(\vec{m})\circ\boldsymbol{g}(x,\vec{m})$ in the second left-hand side term is approximated as $\boldsymbol{g}(x,\vec{m}) - \boldsymbol{K}(\vec{m})\circ \boldsymbol{g}(x,\vec{m}) - \boldsymbol{K}(\vec{m})\circ\boldsymbol{g}(x+\Delta x,\vec{m})$. [A rationale expansion of $\boldsymbol{Q}$ in terms of $\boldsymbol{K}$ avoids this last step, but the exponential form is kept because it is natural from Eq. (2), see below and West *et al*., 1992, p. 33.] One then recovers Eq. (4). Hence, Eq. (6) is an approximate solution of Eq. (4).

Equation (6) is an original result of the present study. It can also be obtained from the separation of the stratification and turbulence components under the small-range step approximation ($k_0\Delta x < 1$), as proposed by Macaskill and Ewart (1984) and Gilbert *et al*. (1990, Appendix) for the first-order moment. In the absence of mean refraction, c_0 is chosen such that $\langle\varepsilon_{mov}\rangle = 0$, and the turbulence-related exponential terms from $\boldsymbol{Q}$ in Eq. (6) are consistent with the analytical results obtained under the Rytov formalism with turbulence only [Ostashev, 1997, p. 201; Wilson *et al*., 2009, Eq. (30)]. In the absence of turbulence, Eq. (6) is equivalent to $\boldsymbol{A}(x+\Delta x,\vec{m}) = \boldsymbol{R}(\vec{m})\boldsymbol{A}(x,\vec{m})$ for the complex amplitude $A(x,z,\vec{m}) = p(x,z,\vec{m})e^{-ik_0x}$. As expected, this is the solution of the first-order moment with mean refraction only [Gilbert and White, 1989, Eq. (8)].

The present model implements Eq. (6) to advance $\boldsymbol{g}$ with range for a fixed θ. In practice, it is an adaptation of the first-order moment model by Gilbert and White (1989). It thus uses the same linear finite elements discretization on the vertical, which is argued to account for the vertical fluctuations with height more smoothly than finite differences. Besides the accounting for turbulence, the major difference is that the present model works with the second-order moment. Accordingly, the parent algorithm to evaluate $\boldsymbol{RA}$ ($\boldsymbol{A}$ is a vector) operates on matrix columns to evaluate Eq. (6), written as $(\boldsymbol{R}(\boldsymbol{R}(\boldsymbol{Q}\circ\boldsymbol{g}))^{*T})^{*T}$. The initial condition is $\boldsymbol{g}(0,\vec{m}) = \boldsymbol{A}_0\boldsymbol{A}_0^{*T}$, with $\boldsymbol{A}_0$ the Gaussian-with-height starter function of Gilbert and White (1989). Below, the model horizontal and vertical grids are taken to be uniform with equal resolutions, and chosen as one tenth the acoustic wavelength ($k_0\Delta x < 1$, as required above). The computational domain height is one third the maximum propagation range.

At the surface, an impedance boundary condition for the amplitude writes as

$$\frac{\partial A(x,z,\vec{m})}{\partial z} = -ik_0\frac{A(x,z,\vec{m})}{Z_b}, \quad (8)$$

where Z_b is the surface complex impedance normalized by a reference density and sound speed. Following Gilbert and White (1989) and West *et al*. [1992, Eq. (49)], Eq. (8) can be implemented by taking the $(1,1)$ matrix coefficient of $\boldsymbol{H}$ as the $(1,2)$ coefficient times $-(1-ik_0\delta z/Z_b)$, with δz the height difference between the first two levels. The present model conforms to this formulation. It uses the so-formed operator $\boldsymbol{R}_{bc}$ in lieu of $\boldsymbol{R}$ in Eq. (8), and includes an additional level just above the first level in order to better resolve this boundary condition. This inclusion is straightforward with finite elements. The upper boundary condition uses an artificial attenuation in the top part of the sound speed profile to damp the propagation.

B. Evaluation

In the evaluation tests below, the meteorological conditions are arbitrarily prescribed, i.e., $\vec{m}$ and θ are fixed through the specification of b_ε and $\langle\varepsilon_{mov}\rangle$ or $\langle c_{mov}\rangle$.

The model has first been tested without turbulence, in the scenarios investigated by Gilbert and White (1989). The source emits at 40 Hz from $z = 2$ m. The normalized ground impedance is $Z_b = 31.4 + i38.5$. The sound speed is $\langle c_{mov}\rangle(z) = c_s + g_c\min(z,h)$, with $c_s = 330\,\mathrm{ms}^{-1}$ and $h = 100$ m. Gilbert and White (1989, Sec. II B) test a wide-angle version of their first-order moment PE model, as obtained from the narrow-angle version with a simple modification in $\boldsymbol{H}$. The present model has first been tested in this wide-angle version. As shown on Fig. 1, the predicted sound levels match the results of Gilbert and White (1989), in both the upward and downward refraction cases ($g_c = -0.12\,\mathrm{s}^{-1}$ and $g_c = 0.12\,\mathrm{s}^{-1}$, respectively). This validates the accounting of the mean refraction and surface boundary condition with the implemented technique of Eq. (6). Comparing with the (narrow-angle) reference version, the impact of the PE angular limitation is found to manifest itself only at ranges beyond 2500 m (Salomons, 1998).

The second test is the upward refraction scenario of Wilson and Ostashev (2001). The source height and frequency are 5 m and 40 Hz. The normalized ground impedance is $Z_b = 20.8 + i\,19.2$. The mean sound speed is $\langle c_{mov}\rangle(z) = c_0 - u_*\ln(\max(z,z_0)/z_0)/k_{vK}$ with $u_* = 0.6\,\mathrm{ms}^{-1}$ and $z_0 = 0.01$ m. Here k_{vK} is the von Karman constant ($k_{vK} = 0.4$). The function b_ε is range-independent, and is parameterized following $b_\varepsilon(z_1,z_2) = 6b_{vK}(\sigma_u^2,l_u,l)/c_0^2$, with

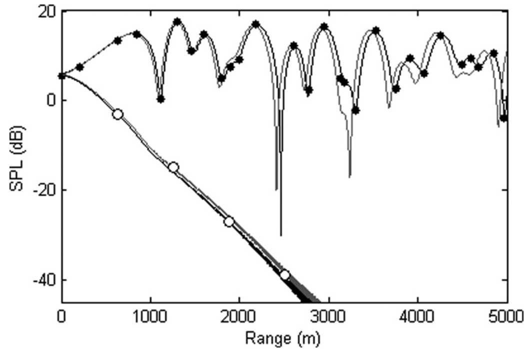

FIG. 1. Relative sound pressure level (SPL) with range at $z = 1$ m. The black and gray lines are with the wide-angle and narrow-angle versions of the present model, respectively. The upper (respectively, lower) data are for downward (respectively, upward) refraction. The symbols show some sampled predictions from Gilbert and White (1989).

$$b_{vK}\left(\sigma_u^2, l_u, l\right) = \frac{8\sqrt{\pi}\sigma_u^2 l_u}{3\Gamma(1/3)}\left(\frac{l}{2l_u}\right)^{5/6} \times \left[K_{5/6}\left(\frac{l}{l_u}\right) - \frac{l}{2l_u}K_{1/6}\left(\frac{l}{l_u}\right)\right]. \quad (9)$$

In Eq. (9), K_α is the modified Bessel function of the second kind, $\sigma_u^2 = 3u_*^2$ scales the intensity of momentum (wind velocity) turbulent fluctuations, $l = |z_2 - z_1|$ and $l_u = 1.8(z_1 + z_2)/2$ is a characteristic scale of turbulence.

Figure 2 shows the sound level prediction with height. The initial decrease near the surface is less abrupt than in the simulation by Wilson and Ostashev (2001). At long ranges, the near-surface sound levels agree in the two models. The discrepancy also appears without turbulence. In the case without turbulence, the Euler equations model of Cheinet and Naz (2006) and the present PE model agree at moderate ranges (this comparison was made for a perfectly reflecting surface). The model by Wilson and Ostashev (2001) notably differs from the present model by the use of finite differences with height and a second-order surface boundary condition. The transverse coherence factor [normalized values of $g(x, z_1, z_2, \vec{m})$ with $z_1 \neq z_2$] has also been compared (not shown). Consistent with the above discrepancy, the present model holds slightly more coherence than the model by Wilson and Ostashev (2001) at moderate ranges, but the agreement is excellent at 2000 m. This suggests that the parameterization of the turbulence scattering with Eq. (6) is reliable.

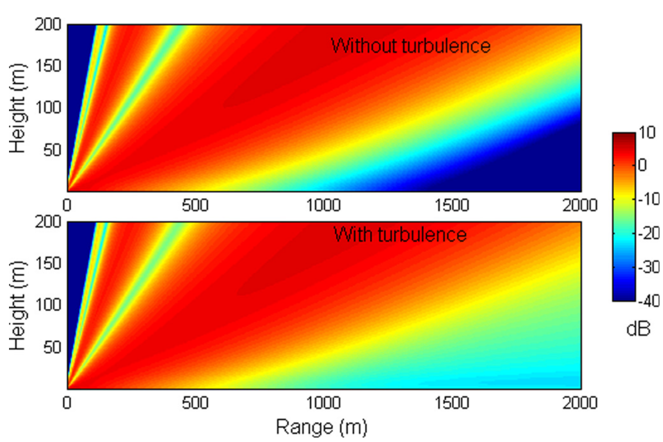

FIG. 2. (Color online) Relative sound pressure level with range and height, without and with turbulence, in the test case of Wilson and Ostashev (2001).

The last test is the idealized case considered by Gilbert *et al.* (1990) and Chevret *et al.* (1996), which is inspired from the measurements by Wiener and Keast (1959). The source height and frequency are 3.7 m and 424 Hz. The normalized ground impedance is $Z_b = 8 + i9.24$. The mean sound speed is $\langle c_{mov}\rangle(z) = c_0 - a\ln(\max(z, z_0)/d)$, where a is a velocity scale, $c_0 = 340\,\mathrm{ms}^{-1}$, $d = 0.006$ m, and $z_0 = 0.01$ m. The function b_ε is range-independent, and is parameterized from Gilbert *et al.* [1990, see also Wilson, 1998, Eq. (43)]:

$$b_\varepsilon(z_1, z_2) = \sqrt{\pi}\sigma_\varepsilon^2 l_\varepsilon \exp\left(-\frac{l^2}{l_\varepsilon^2}\right), \quad (10)$$

where $\sigma_\varepsilon^2 = 2 \times 10^{-6}$ scales the intensity of turbulence fluctuations, $l = |z_2 - z_1|$ and $l_\varepsilon = 1.1$ m is a characteristic scale of turbulence.

Figure 3 shows the sound levels at $z = 1.5$ m in two cases, of strong upward refraction ($a = -2\,\mathrm{ms}^{-1}$) and weak upward refraction ($a = -0.5\,\mathrm{ms}^{-1}$). In both cases, the model predictions generally agree with the predictions by Chevret *et al.* (1996) and Gilbert *et al.* (1990). As discussed by Wilson (2000), some prescriptions are required in modeling the atmospheric conditions in this test case, for which no observational data are available. Therefore it is not too surprising that the predictions do not match the observations of Wiener and Keast (1959), here shown for reference. Still, there is a non-negligible scatter between the models. Chevret *et al.* (1996) and Gilbert *et al.* (1990) use a different method to diagnose the sound levels: they average some propagation simulations through a number of 2D distributions of ε_{mov}. Other differences between the models may relate to the starter field (e.g., presence of the ground-reflected component), the boundary conditions (e.g., formulation of the impedance condition) and the arbitrary sound level reference.

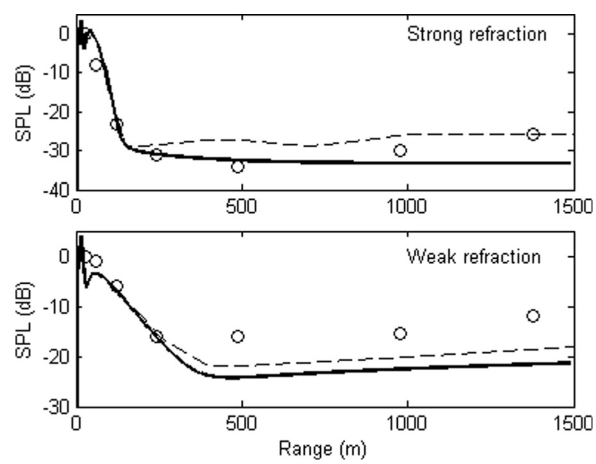

FIG. 3. Relative sound pressure level (SPL) with range at $z = 1.5$ m, predicted by the present model (full lines) and by Chevret *et al.* (1996, dashed lines), in the strong and weak upward refractive conditions of Gilbert *et al.* (1990). The symbols are the observations by Wiener and Keast (1959).

III. ATMOSPHERIC MODEL

In the sound propagation model of Sec. II, the atmosphere is felt through $\langle \varepsilon_{mov} \rangle (z, \vec{m})$ and $b_\varepsilon(x, z_1, z_2, \vec{m})$. This section discusses a parameterization for these quantities in the lower atmosphere in terms of well-defined meteorological factors.

A. Driving meteorological factors

It is known that the structure of the surface layer is largely impacted by the dynamical and thermo-dynamical production terms for momentum turbulence. The friction velocity u_* scales the dynamical production near the surface. It varies with the near-surface wind, and ranges in the interval $0.01 - 1\,\mathrm{ms}^{-1}$. Conversely, the surface buoyancy flux F_b scales the thermal stabilizing/destabilizing effect of the surface. Although humidity contributes to buoyancy, the approximation $F_b \approx F_T$ is appropriate to the purpose of this study (Appendix A), where F_T is the kinematic surface flux of temperature. Over land, F_T is typically positive ($0.2 - 0.5\,\mathrm{Kms}^{-1}$) on fair-weather days (ground warmer than air) and negative ($-0.1\,\mathrm{Kms}^{-1}$) on clear nights (e.g., Cheinet *et al.*, 2005). Denoting γ the gravity constant, the balance between buoyancy- and shear-driven production terms defines the Obukhov length:

$$L = -u_*^3 T_0 / (k \gamma F_b). \tag{11}$$

Monin-Obukhov Similarity (MOS) assumes that u_* and F_b are the sole meteorological forcings of the surface layer structure. There are major restrictions for MOS to hold. First, MOS applies in the surface layer, in which the surface fluxes are relatively constant. This layer may be 200 m thick under unstable conditions, but may be considerably thinner under very stable conditions. The turbulence must be in a quasi-stationary regime. Again, this implies the failure of MOS under very stable conditions, say $z/L > 2$, in which case the turbulence is highly intermittent. If the atmospheric levels which predominantly affect the sound propagation are below 200 m, the condition writes as $L > 100$ m. For illustrative purposes, this condition is extended to $L > 20$ m. Besides, the surface must be homogeneous. Fetch effects, mountainous or coastal environments can not be described. Wind turning with height and low-level inversions (changes in the signs of the gradients) are also not accounted for. Last, MOS is valid in an ensemble-average sense. *In situ* tests use temporal averages over tens of minutes, and the average $\langle \rangle$ should be defined accordingly.

Despite these limitations, MOS offers a general, physically based, well-documented description of the surface layer properties. In that respect, it is considered one robust result of contemporary meteorology. It is commonly used in operational numerical weather prediction systems (Beljaars, 1994; Cheinet *et al.*, 2011) and in sound propagation numerical studies, among many others. MOS is therefore used in the present study. Accordingly, the vertical profiles of the temperature- and velocity-related fields in the surface layer scale with u_*, F_T, the height z and z/L. Hence the meteorological driving factors are defined as $\vec{m} = (u_*, F_T)$. The use of MOS implies that the turbulence statistics are homogeneous in the horizontal plane. Physically, the large-scale intermittency effects are not described in the present approach (Cheinet, 2008). Accordingly, all turbulence-related quantities hereafter ignore the dependence on x.

B. Parameterization of the atmospheric properties

To model b_ε and $\langle \varepsilon_{mov} \rangle$, the temperature and velocity fluctuations are assumed to be uncorrelated. From the acoustical point-of-view, the velocity fluctuations largely dominate when present. The approach accounts for the temperature contributions under very low winds. The non-correlation is a theoretical requirement in the inertial-convective range (Tatarski, 1961, p. 267). It fails at large turbulence scales, at which the surface layer dynamics organize (Cheinet, 2003). From this assumption and Eq. (1), one has [Wilson and Ostashev, 2001, Eq. (6)]

$$\langle \varepsilon_{mov} \rangle (z, u_*, F_T) = -\frac{\langle T \rangle (z, u_*, F_T) - T_0}{T_0} - 2\frac{\langle u \rangle (z, u_*, F_T) \cos\theta}{c_0}, \tag{12a}$$

$$b_\varepsilon(z_1, z_2, u_*, F_T) = \frac{1}{T_0^2} b_T(z_1, z_2, u_*, F_T) + \frac{4}{c_0^2} b_u(z_1, z_2, u_*, F_T). \tag{12b}$$

Second, the temperature and momentum fluctuations are assumed to be isotropic, and are parameterized with a von Karman model. It is recognized that anisotropy generally affects the wind fluctuations (Appendix C). The treatment of anisotropy however precludes a closed-form treatment of the projected correlation function (Wilson, 2000). For the von Karman model, one has (Appendix B)

$$b_T(z_1, z_2, u_*, F_T) = b_{vK}\left(\sigma_T^2(z_h, u_*, F_T), l_T(z_h, u_*, F_T), \Delta z\right), \tag{13a}$$

$$b_u(z_1, z_2, u_*, F_T) = \frac{3}{2} b_{vK}\left(\sigma_u^2(z_h, u_*, F_T), l_u(z_h, u_*, F_T), \Delta z\right), \tag{13b}$$

where $\Delta z = |z_2 - z_1|$ and $z_h = (z_1 + z_2)/2$. The function b_{vK} was introduced in Eq. (9). Here σ_T^2, σ_u^2, l_T and l_u are the variances and outer scales of temperature and momentum turbulent fluctuations. As discussed in Appendix B, the outer scales in the von Karman model can be parameterized according to

$$l_T(z, u_*, F_T) = \left(2.34\sigma_T^2(z, u_*, F_T)/C_T^2(z, u_*, F_T)\right)^{3/2}, \tag{14a}$$

$$l_u(z, u_*, F_T) = \left(1.91\sigma_u^2(z, u_*, F_T)/C_u^2(z, u_*, F_T)\right)^{3/2}, \tag{14b}$$

where C_T^2 and C_u^2 are the structure parameters of temperature and momentum fluctuations.

The present study uses the following parameterization. For a couple (u_*, F_T), L is calculated with Eq. (11), and the vertical profiles of $\langle T\rangle$, $\langle u\rangle$, σ_T^2, σ_u^2, C_T^2 and C_u^2 are calculated with the MOS flux-profile relationships in Appendix C. Equations (12), (13), and (14) allow deriving the vertical profile of $\langle \varepsilon_{mov}\rangle$ and the dependence of b_ε on (z_1, z_2). The vertical grid in this parameterization is the grid of the sound propagation model, so the diagnosed $\langle \varepsilon_{mov}\rangle$ and b_ε can be directly ingested by the latter model.

The MOS relationships do not apply at heights of the order of the surface roughness length z_0, which scales the surface irregularities on the vertical. At these levels, the wind and the bi-dimensional correlation functions for temperature and momentum are taken to be null. The temperature is interpolated from the temperature at $z = 1$ m with the MOS temperature gradient at $z = 0.5$ m. Besides, C_T^2 and σ_T^2 have no well-defined MOS behavior near neutrality. This may introduce an upper bound for $|L|$. However, the temperature fluctuations are small near neutrality, so it is sufficient that the expressions yield $b_T \approx 0$ in Eq. (13a), as discussed in Appendix C.

Wilson (2000) parameterizes b_u from two independent, shear-driven and buoyancy-driven contributions. The present parameterization assumes a single von Karman model for b_u. It yields the same results in the asymptotic neutral and purely convective conditions (Appendix C). The applicability of the present approach to stable conditions is an original addition compared to Wilson (2000), but it restricts to regimes under which MOS is applicable.

In the illustrative simulations below, z_0 is set to 0.01 m. Figure 4 shows the near-surface vertical gradient of $\langle c_{mov}\rangle$, which directly informs on the sign and strength of the mean refraction. Three azimuthal directions are considered. The refraction is upward in the upwind direction. In the crosswind direction, the refraction is only temperature-driven, i.e., it follows stability. Downwind, the wind tends to refract the sound downward, but the refraction is still upward under low winds and strong surface heating. These results are consistent with those of Wilson (2003), also obtained under MOS.

Figure 5 shows $\sigma_u^2 l_u / c_0^2$, which weights the wind-induced turbulence when $z_1 = z_2$ [Eqs. (13b) and (9)]. This quantity strongly varies with height, especially under stable conditions. Under unstable conditions below $z = 10$ m, it decreases as u_* increases. Physically, the moderate increase of total fluctuations (σ_u^2) is concomitant with a large increase of small-scale fluctuations (C_u^2), so the larger-scale fluctuations (l_u) decrease. The height $z = 50$ m is representative of the effective atmospheric levels for sound scattering (Fig. 2). The quantity $\sigma_u^2 l_u / c_0^2$ at this height is strongest under stable conditions. Under unstable conditions, it expectedly increases with the surface heat and momentum forcings. The temperature-induced turbulence (not shown) is non-negligible only below $z = 10$ m, and it never exceeds the wind-driven component.

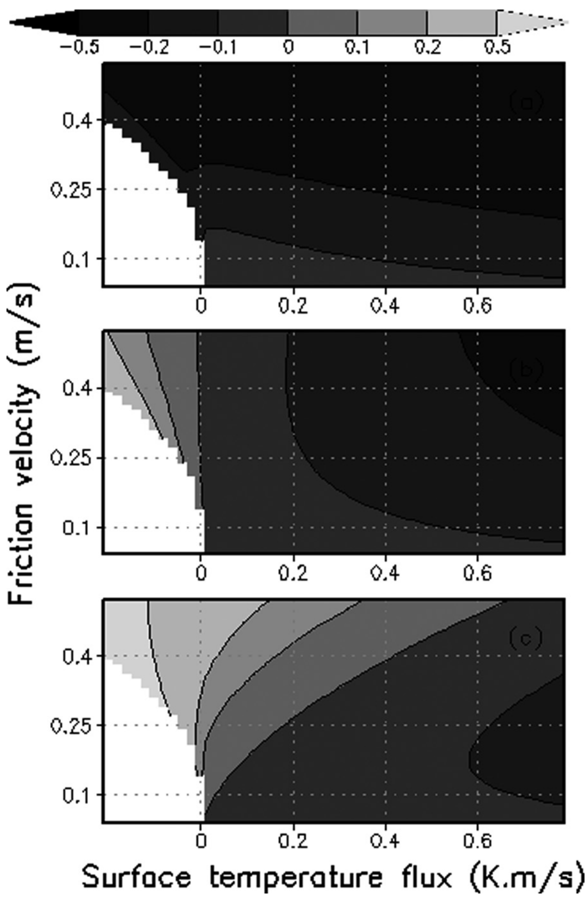

FIG. 4. Vertical gradient of the effective sound speed (s^{-1}) at $z = 3.5$ m with the surface temperature flux F_T and the friction velocity u_*, (a) upwind, (b) crosswind, and (c) downwind. Calculations are not shown where the Obukhov length is smaller than 20 m.

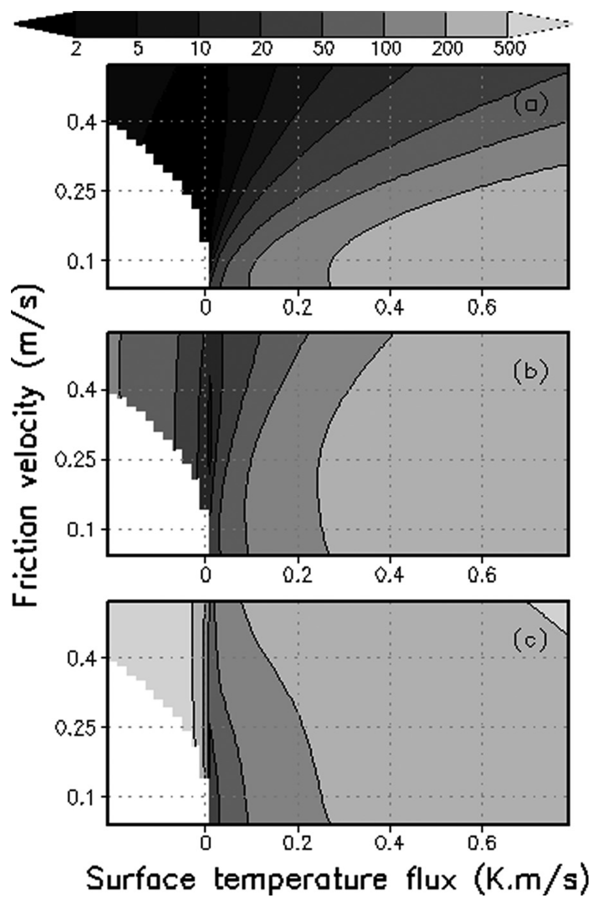

FIG. 5. Wind-induced turbulence, quantified by $10^5 \sigma_u^2 l_u / c_0^2$ (m) with the surface temperature flux F_T and the friction velocity u_*, at (a) $z = 1$ m, (b) $z = 10$ m, and (c) $z = 50$ m.

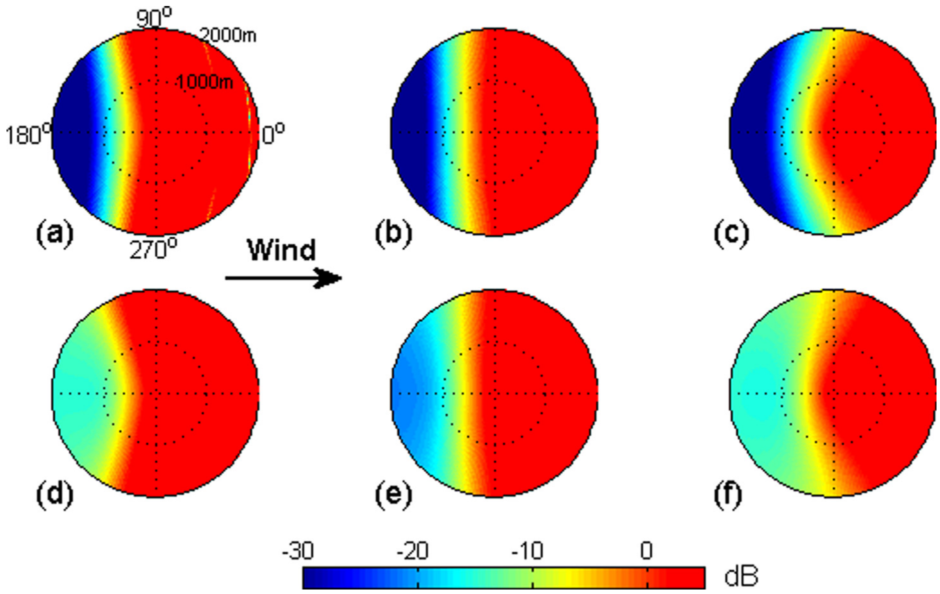

FIG. 6. (Color online) Relative sound pressure level at $z = 1$ m with range and propagation angle [see (a)], in presence of a moderate Easterly wind ($u_* = 0.5\,\mathrm{ms}^{-1}$), as simulated (top) without turbulence and (bottom) with turbulence. The thermal stability is (a) and (d) stable ($F_T = -0.1\,\mathrm{Kms}^{-1}$), (b) and (e) quasi-neutral ($F_T = 0.01\,\mathrm{Kms}^{-1}$), and (c) and (f) unstable ($F_T = 0.4\,\mathrm{Kms}^{-1}$).

These results are consistent with those by Ostashev and Wilson (2000, Fig. 1).

The parabolic equation approach requires that the acoustic wavelength be shorter than the characteristic scale l_{tot} of the medium fluctuations (Clifford and Lataitis, 1983; Ostashev, 1997, p. 195). This may be seen as a high-frequency limitation or alternatively as a lower bound on the turbulence scales which may be accounted for. The lowest frequency used hereafter is 40 Hz. The dominance of wind fluctuations suggests using $l_{tot} \approx l_u$. The condition can then be expressed as $l_u > 9$ m. It has been checked that, in the present parameterization, this condition is largely fulfilled above $z = 10$ m whatever the atmospheric forcings. For example, at $z = 50$ m, l_u is always greater than 100 m. Under upward refractive conditions, of interest to this study, the levels of significant sound pressure and turbulence levels (i.e., of significant turbulent scattering) are located well-above $z = 10$ m (Figs. 2 and 5). Hence, the application of the parabolic equation approach is appropriate to the present purpose of sound level diagnostics in the refractive shadows. In neutral or downward refracting conditions, the sound levels are determined by the mean refraction—except in the interference fringes. The present approach is thus also appropriate in these cases.

IV. SOUND LEVELS IN REFRACTIVE SHADOWS

This section uses the above developments to investigate the sound levels in presence of mean refraction and turbulent scattering. Given a scenario (source height and frequency, surface type), the approach works as follows. The input parameters are the meteorological factors (u_*, F_T) and the propagation angle θ. From these input conditions, the near-surface refractive properties $\langle \varepsilon_{mov} \rangle$ and b_ε are derived following Sec. III, and are passed to the numerical model of Sec. II. This model makes a prediction of the sound levels with range and height in the considered conditions.

Because MOS is valid only in the surface layer, the approach is limited to near-surface sound propagation. Some preliminary tests confirm the rule-of-thumb according to which the atmospheric heights of relevance to sound propagation amount to a tenth of the range. With the surface layer height limited to 200 m, the approach is not valid at larger ranges than 2000 m. On the other hand, the present parameterizations of the atmospheric stratification and turbulence are both based on the MOS formalism. This consistency is deemed of primary importance, because it captures the wind-dependent, stability-dependent correlation between the stratification and turbulence properties.

The following illustrative acoustic scenario is considered. The source frequency and height are 40 Hz and 2 m. A grass-covered surface is assumed. Accordingly, the roughness length is set to $z_0 = 0.01$ m and the normalized ground impedance to $Z_b = 31.4 + i38.5$. The vertical and range resolutions of the model are set to 1 m. The sound levels are diagnosed at $z = 1$ m.

A. Width of the shadow zones

Figure 6 illustrates the near-surface sound levels in the presence of several stratification conditions, first ignoring turbulence [i.e., $b_\varepsilon = 0$ in Figs. 6(a)–6(c)]. Each panel is formed from 180 model runs, with an every-degree-scan over θ (Eq. (1) is symmetric with $-\theta$). The friction velocity is set to $u_* = 0.5\,\mathrm{ms}^{-1}$, and F_T varies from negative to positive values from panel to panel. Well-defined shadow zones are formed in the upwind directions, even in stable conditions, favorable to downward refraction. Turbulence is accounted for in the lower panels. No relative sound level below -21 dB is obtained with turbulence scattering. Hereafter, the range 1500 m is selected to analyze the shadow zone. The shadowing is well-marked at this range, i.e., the diffractive effects do not contribute much to the observed sound levels (see Fig. 2). Besides, this range remains within the domain of validity of the approach.

Hereafter the shadow zone is defined as the area in which the relative sound level is less than the free-field reference, i.e., approximately 4 dB in the present simulations. Figure 6 shows that this diagnostic takes the form of an angular sector centered at the source position (Wiener and

TABLE I. Shadow zone angular width under various atmospheric forcings, according to the model predictions and to the analytical prediction of Eq. (15).

	$F_T = -0.1$ Kms^{-1}	$F_T = 10^{-2}$ Kms^{-1}	$F_T = 0.2$ Kms^{-1}	$F_T = 0.4$ Kms^{-1}
Present model	150°	180°	210°	234°
Eq. (15)	152°	180°	234°	298°

Keast, 1959, Fig. 1). Table I gives the corresponding shadow zone width (i.e., angular aperture of relative sound levels lower than 4 dB at 1500 m). As expected, the shadow zone widens under more unstable conditions. The aperture prediction without turbulence never exceeds the prediction with turbulence by more than 10°. Hence, the turbulence scattering hardly alters this so-defined shadow zone width.

An analytical evaluation of the shadow zone angular width may be obtained under the assumption that the receiver and the source are at the same height z. Then the shadow zone boundary is the propagation direction θ_c at which the effective sound speed gradient vanishes. Applying MOS relationships gives

$$\cos(\theta_c(z, u_*, F_T)) = -\frac{c_0}{2T_0}\frac{\left(\dfrac{\partial T}{\partial z}\right)_z}{\left(\dfrac{\partial u}{\partial z}\right)_z} = -\frac{c_0}{2T_0}\frac{T_*\varphi_h(z/L) + \kappa z\Gamma_d}{u_*\phi_m(z/L)}, \qquad (15)$$

where T_*, Γ_d and the dimensionless functions $\phi_{m,h}$ are defined in Appendix C. The second relation is strictly equivalent to Wilson [2003, Eq. (19)]. The shadow zone angular width is $2\pi - 2\theta_c$. When the receiver and source are not at the same height, Wiener and Keast [1959, Eq. (1)] propose to use Eq. (15) with z taken as half the average height of the receiver and source, i.e., 0.75 m in the present scenario. Table I gives the shadow zone angular width calculated with this method. It shows the same sensitivity to stability as the present predictions. However, this method does not provide a comparable quantitative estimate under strongly unstable conditions.

B. Depth of the shadow zones

The upwind propagation ($\theta = 180°$) informs on the minimum sound level at a given range, i.e., on the shadow zone depth. The analysis is performed for u_* and F_T discretely scanned with 50 linearly spaced values each. It thus uses 2500 simulations, each of which is used to calculate the sound level at the range 1500 m and height 1 m.

Figure 7(a) shows the upwind sound levels in terms of the atmospheric forcings, as predicted without turbulence. The overall picture is driven by the adverse wind: the stronger u_*, the lower the sound levels. More unstable conditions expectedly deepen the shadow zone. However, near neutrality, the sound levels are lower under stable than under unstable stratification. This result reflects that the wind stratification, which has a prevalent role, rapidly strengthens as the surface heat flux becomes negative. The visual effect is a low level tongue under moderately stable conditions ($F_T \approx -0.05$ Kms^{-1}).

Figure 7(b) is the main result of this study. It gives the upwind shadow zone sound levels in presence of turbulence scattering. According to it, turbulence only plays a minor role under conditions with very low (positive) heat flux and very low winds, because the turbulence intensity is itself small (Fig. 5 at $z = 50$ m). Except in this case, the impact of turbulence is non negligible, and it is dramatically important for non-small values of the wind forcing ($u_* > 0.35$ ms^{-1}). In a general sense, turbulence enhances the shadow zone

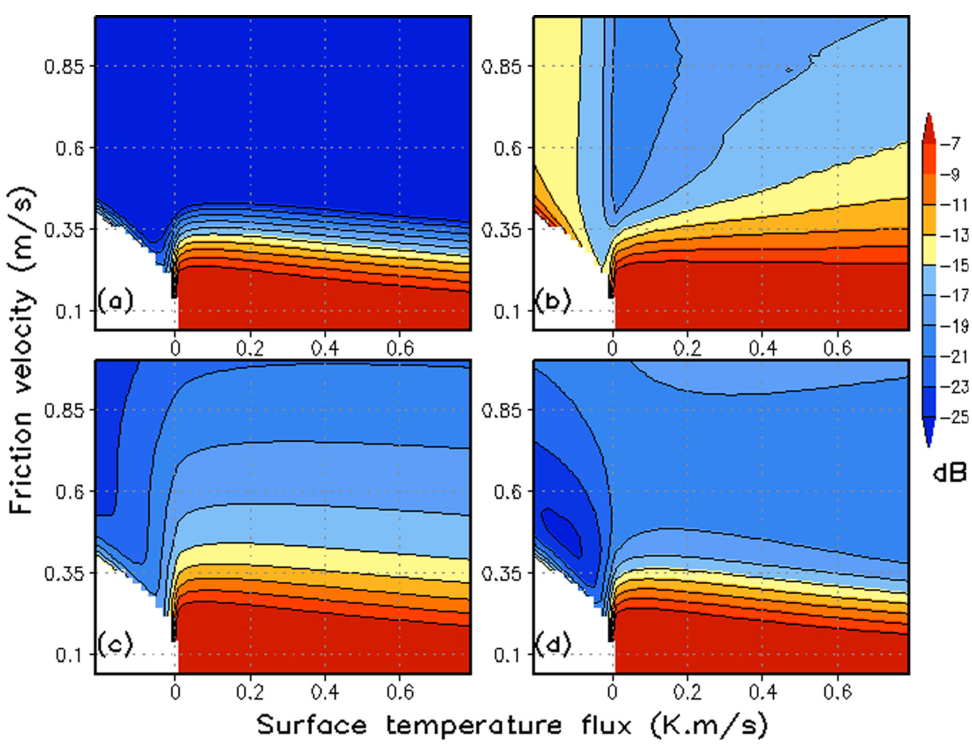

FIG. 7. (Color online) Relative sound pressure level in the upwind direction at $z = 1$ m, with the surface temperature flux F_T and the friction velocity u_*, (a) without turbulence, levels below −25 dB are not shown, (b) with the reference turbulence model, (c) with fixed turbulence, and (d) with neutral-atmosphere turbulence.

sound levels. Beyond this expected result, the predictions reveal some aspects of the sensitive balance between the mean refraction and turbulent scattering. In that respect, three major lessons emerge from Fig. 7(b).

1. The upwind sound levels tend to decrease with the surface momentum forcing (u_*) under unstable conditions. This sensitivity is caused by the enhanced mean refractive effect of a larger adverse wind gradient. According to the present predictions, this effect prevails over the enhanced turbulence rate, which concurrently tends to enhance the sound levels. The strong decrease of the sound levels with increasing winds under very stable conditions is subject to caution given the limitations of MOS in these situations.
2. In a transition from unstable to stable conditions with constant u_*, the wind rapidly strengthens, which increases the mean refraction and tends to decrease the upwind sound levels [Figs. 4 and 7(a)]. However, the acoustically-effective turbulence also strongly increases (Fig. 5). According to the present simulations, the turbulence scattering effects prevail, and the upwind sound levels slightly increase in this transition. The reversed physics would occur in a transition from stable to unstable conditions. As a result of the enhanced turbulence scattering under stable conditions, the low sound level tongue of Fig. 7(a) is attenuated in Fig. 7(b).
3. As the surface heat flux increases from moderately to strongly unstable conditions (e.g., in the morning over land with fair weather), the enhanced thermal instability tends to decrease the upwind sound levels [Figs. 4 and 7(a)]. On the other hand, the turbulence enhancement (Fig. 5) tends to increase the sound levels. The present predictions suggest that the turbulence scattering effects again prevail in this transition under non-small values of the wind forcing. The reversed physics would occur in the late afternoon over land.

Hence, the upwind sound levels tend to increase with the absolute value of the surface heat forcing, as this sensitivity is driven by the refractive turbulence. From the different panels in Fig. 6, this tendency can be generalized to other propagation angles within the shadow zones. Conversely, the sound levels tend to decrease with the surface momentum forcing, as this sensitivity is driven by the mean refraction, at least under unstable conditions. This is to our knowledge the first systematic analysis of the sensitivity of the shadow zone sound levels to the meteorological conditions.

C. Parameterization of shadow zone sound levels

As previously discussed, the development of sound level parameterizations in the shadow zones is an important challenge in outdoor acoustics. Some parameterizations proposed in the literature are now discussed.

Wiener and Keast (1959, Fig. 5) parameterize the shadow zone sound levels in terms of the angular distance between the considered propagation direction and the shadow zone boundary. The qualitative trend they obtain, of lower sound levels at larger angular distances, is confirmed in the present simulations (Fig. 6). However, Fig. 6 also suggests that the sound level varies by more than 7 dB according to the meteorological conditions, for a same angular distance from the boundary. The trend inferred by Wiener and Keast is of the same order at large angular distances from the boundary, so it could be impacted by their sampling of the atmospheric conditions.

As discussed in Sec. I, a practical method to account for turbulence scattering is to set an empirical minimum on the relative sound level calculated without turbulence. The prescription of van Maercke and Defrance (2007) and Salomons *et al*. (2011) gives a minimum of -20.5 dB in the selected configuration. Figure 7(a) may be seen as following this method with a -25 dB minimum. This approach ignores the impact of turbulence when the sound level prediction without turbulence is above the threshold. Figure 7(b) suggests that turbulence may enhance the sound levels by more than 5 dB for sound levels larger than -10 dB. The above approach also ignores the sound level variations when the prediction without turbulence is below the threshold, i.e., deep in the shadow. Again, Fig. 7(b) suggests that the sound levels vary by more than 5 dB according to (u_*, F_T).

The sensitivity of the sound level predictions to the turbulence parameterization can also be assessed. First, the refractive index structure parameter and the outer scale are set independent of the meteorological forcings. Here only momentum fluctuations are considered, with $l_u = 50$ m (Wilson and Ostashev, 2001) and $\sigma_u^2 = 0.058\,\mathrm{m}^2\mathrm{s}^{-2}$, which yields $\sigma^2_{\varepsilon,mov} = 2 \times 10^{-6}$ (Daigle, 1979). As shown in Fig. 7(c), this setting does not reproduce the sensitivity of enhanced sound levels under more unstable conditions, as simulated with the present, more physical turbulence parameterization. Another approach is to only account for the wind-driven dependence of the turbulence properties, while ignoring the sensitivity to buoyancy. Specifically, C_u^2 and σ_u^2 are given their neutral asymptotes ($3.9u_*^2/z^{2/3}$ and $3u_*^2$, respectively), which implies $l_u = 1.8(z_1 + z_2)/2$. Figure 7(d) shows that the resulting predictions do not capture the sound levels enhancement under more unstable conditions. They also predict a deeper shadow zone under stable conditions.

These sensitivity tests show that the feedback between the meteorological forcings and the turbulence properties is a key component in determining the sound characteristics in near-surface shadow zones.

V. CONCLUSIONS

The outdoor sound propagation strongly depends on the atmospheric conditions through the mean refraction and the turbulent scattering. The mean upward refraction results in extremely low sound levels, thereby forming a so-called refractive shadow zone. The turbulence scattering causes the penetration of sound into the shadow zones. The sound levels in the shadow zones thus result from a complex balance between the refractive effects of the mean and turbulent fluctuations. Quantifying this balance requires the formulation of a consistent model of (1) the atmospheric stratification, (2) the atmospheric turbulence, and (3) their impact on sound propagation. In the last decade, some solutions have been formulated to address these issues separately. The present study couples these formulations to systematically analyze the sound level predictions in refractive shadow zones.

The approach uses the well-evaluated framework of Monin-Obukhov Similarity (MOS) to describe the atmospheric stratifications in wind and temperature. Humidity is not included, since over land, its effects can be inferred from the results without it. The input parameters are two standard meteorological quantities, namely the friction velocity and the kinematic surface flux of temperature. The use of MOS restricts the approach to near-surface propagation, with an implied range limitation of the order of 2000 m. It also limits the validity of the approach under very stable conditions (e.g., clear nights over land). Momentum and temperature turbulent fluctuations are parameterized with von Karman isotropic spectral models. The free parameters of the spectra are taken as the structure parameter and the variance. The closures for these quantities also use MOS relationships, in consistency with the stratification derivation. The analysis shows that the acoustically effective turbulence is almost always driven by the wind fluctuations.

The sound propagation model ingests the above-prescribed stratification and turbulence properties. It numerically solves a second-order moment Parabolic Equation (PE) in two dimensions (range, height), obtained under the narrow-angle propagation approximation. Under a small range step approximation, an original implementation is introduced, which requires only minor modifications to a first-order moment PE model. The PE approach requires that the characteristic scale of the turbulent fluctuations be larger than the acoustic wavelength. This condition is found to be valid at the considered frequencies (down to 40 Hz). The model is evaluated in previously documented cases. The present predictions are within the range of uncertainty of the other models, for the sound level as well as for the coherence factor. An inter-comparison could be useful to ascertain the origin of the differences between the predictions by various models.

The so-formed atmospheric-acoustic coupled model allows for the investigation of the sound field characteristics in refractive shadow zones. An illustrative acoustic scenario is selected. The concept of an angular boundary for the shadow zone is shown to hold, beyond which the sound levels are lower than the free-field value. The approach reproduces the expected increase of the shadow zone sound levels in the presence of turbulent scattering. It also provides the first systematic, quantitative assessment of the balance between the effects of the mean refraction and turbulent scattering in determining the shadow zone sound levels. The emerging picture is that the sound levels tend to increase with the absolute value of the surface heat forcing, as this sensitivity is driven by the turbulent scattering. Conversely, the sound levels tend to decrease with the surface momentum forcing, as this sensitivity is driven by the adverse mean refraction, at least under unstable conditions.

Formulations proposed in the literature to parameterize the shadow zone sound levels have been investigated. Simplified formulations of the turbulence properties have also been tested. These formulations are generally not capable of reproducing the sensitivities predicted with the full coupled approach. Differences with the present sound level estimates may be larger than 5 dB according to the meteorological conditions. A careful assessment of the turbulence properties and effects is necessary if one aims at a more reliable prediction of the sound levels in refractive shadows.

The present results hold for a specific acoustic scenario: source height and frequency, surface type, height of analysis. The sensitivity of the shadow zone sound levels to these parameters could be assessed with the present method, but it is difficult to anticipate on the basis of the present results. For example, the sound frequency determines the strength of the diffractive effects as well as the relevant sizes of turbulent fluctuations and therefore their intensity. There may also be some limitations in such a sensitivity analysis. The sound frequency directly monitors the model vertical and horizontal resolutions. Tests of the approach at high frequencies may thus raise some computational limits. The low frequency counterpart may be bounded by physical limitations in the approach (1) from the parabolic equation approximation, and (2) from the approximation that the relevant turbulent fluctuations are locally homogeneous and isotropic.

The present approach relies on standard, consistent assumptions in atmospheric and acoustic sciences. The experimental evaluation of the results would be a strong consistency check of these assumptions. At present, only few experimental data are available to support model predictions in the refractive shadow zones. The reference datasets of Wiener and Keast (1959) and Parkin and Scholes (1964, 1965) are far from complete on the atmospheric side. Sound propagation experiments with a concurrent, updated assessment of the refractive conditions (stratification, turbulence) are certainly needed. The present results provide some physical guidelines as to what key parameters and sensitivities need to be investigated.

ACKNOWLEDGMENTS

This study was trustfully supported by the German Department of Defence through RDir'in Ch. Korff. The author thanks the two anonymous reviewers, K. Wilson (ERDC/CRREL), L. Ehrhardt, S. Hengy and P. Naz (ISL) for their comments on this manuscript. M. White (ERDC/CERL) passed the original model of Gilbert and White (1989) to ISL.

APPENDIX A: HUMIDITY CONTRIBUTIONS

A first contribution of humidity is that the buoyancy flux is $F_b = F_T + \mu T_0 F_q$ in the Obukhov length, with $\mu = 0.607$. This correction usually amounts to several percents. According to Wilson (2003, p. 753), it can be neglected.

The sound speed also depends on the specific humidity q, so one should replace T by $T_c = T(1 + \eta q)$ in ε_{mov}, with $\eta = 0.511$ [Ostashev, 1997, Eq. (6.23)]. The vertical profile of $\langle q \rangle$ could be parameterized following MOS. The humidity structure parameter, humidity variance and the correlation between temperature and humidity turbulent fluctuations are also MOS-compliant (Frederickson *et al.*, 2000). Therefore, the effects of humidity can, in principle, be accounted for in the present method.

The MOS relationships are the same for σ_T^2 and σ_q^2, and for C_T^2 and C_q^2. Thus, the ratio of the contributions of humidity and temperature contributions to b_ε is $\eta^2 C_q^2 T_0^2 / C_T^2$

$= \eta^2 q_*^2 T_0^2/T_*^2 \approx 0.004\beta^{-2}$, irrespective of stability (Appendix B). The Bowen ratio β (surface sensible vs latent heat fluxes) ranges from 5 over semi-arid regions to 0.1 over the sea. Hence, the humidity turbulent fluctuations can be neglected except over the ocean. This result complements the suggestion by Ostashev (1997, Sec. 6.2.7). It does not apply above the surface layer (e.g., Cheinet and Cumin, 2011).

As a summary, in the case of sound propagation over land, it can be approximated that humidity only enters the problem through $\langle T_c \rangle$ replacing $\langle T \rangle$.

APPENDIX B: THE PROJECTED CORRELATION FUNCTION

This appendix is intended to define the function $b_\varepsilon(x, z_1, z_2, \vec{m})$ and model it in terms of standard turbulence quantities.

Let s be a passive conservative scalar. Let $\vec{R}$ and $\vec{R}_0$ be some 3D vectors. The 3D auto-correlation function is $B_s(\vec{R}, \vec{R}_0, \vec{m}) = \langle s'(\vec{R}, \vec{m}) s'(\vec{R} + \vec{R}_0, \vec{m}) \rangle$ with $s' = s - \langle s \rangle$. The 3D spectrum of s, noted $\Phi_s(\vec{R}, \vec{\kappa}_0, \vec{m})$, is the Fourier transform of $B_s(\vec{R}, \vec{R}_0, \vec{m})$. Let $\vec{R}_0 = (x_0, \vec{l}_0)$, with $\vec{l}_0$ in the plane perpendicular to the x axis. The projected correlation function on x axis follows the equivalent relations:

$$b_s(\vec{R}, \vec{l}_0, \vec{m}) = \int_{-\infty}^{\infty} B_s\left(\vec{R}, \left(x_0, \vec{l}_0\right), \vec{m}\right) dx_0, \tag{B1a}$$

$$b_s(\vec{R}, \vec{l}_0, \vec{m}) = 2\pi \int_{-\infty}^{+\infty} \int_{-\infty}^{+\infty} \Phi_s(\vec{R}, (0, \vec{\kappa}_{0\perp}), \vec{m}) e^{i\vec{\kappa}_{0\perp}.\vec{l}_0} d^2\vec{\kappa}_{0\perp}. \tag{B1b}$$

For sufficiently high acoustic frequencies, the atmospheric fluctuations of relevance to scattering are in the inertial-convective range (typically 1 cm to 10 m sizes). Observational evidences suggest that these fluctuations are approximately isotropic and homogeneous. The theory of turbulence then gives:

$$\Phi_s(\vec{R}, \kappa, \vec{m}) = 0.033 C_s^2(\vec{R}, \vec{m}) \kappa^{-11/3}. \tag{B2}$$

Here C_s^2 is the local structure parameter of s, and the numerical coefficient is introduced for consistency with the atmospheric literature (e.g., Cheinet and Siebesma, 2009). For lower acoustical frequencies, the relevant eddies are of larger size (low κ), and their behavior is difficult to parameterize. A standard way to obtain a non-divergent model is to introduce an outer scale l_s which bounds the inertial-convective range. In these lines, the von Karman three-dimensional isotropic spectrum is

$$\Phi_{vK}(\vec{R}, \kappa, \vec{m}) = \frac{1}{4\pi\kappa^2} 0.968 \sigma_s^2(\vec{R}, \vec{m}) \times \frac{\kappa^4 l_s^5(\vec{R}, \vec{m})}{\left(1 + \left(\kappa l_s(\vec{R}, \vec{m})\right)^2\right)^{17/6}}. \tag{B3}$$

The integral of $4\pi\kappa^2$ times Eq. (B3) over $\kappa = [0, \infty)$ gives σ_s^2 as the variance of s. In the inertial-convective range ($\kappa \gg 2\pi/l_s$), Eq. (B3) yields the $-11/3$ power law of Eq. (B2), so C_s^2, l_s and σ_s^2 relate. Equation (14a) is given by Wilson [1998, Eq. (69)].

After Wilson [1998, Eq. (63) multiplied by 2π], the above scalar von Karman model gives $b_s(\vec{R}, l_0, \vec{m}) = b_{vK}(\sigma_s^2(\vec{R}, \vec{m}), l_s(\vec{R}, \vec{m}), l_0)$, with b_{vK} defined in Eq. (9). In a two-dimensional problem, one may introduce $\vec{R} = (x, z)$ to obtain

$$b_s(x, z, l_0, \vec{m}) = b_{vK}(\sigma_s^2(x, z, \vec{m}), l_s(x, z, \vec{m}), l_0). \tag{B4}$$

In presence of large-scale inhomogeneity, Eq. (B4) implies that the projected correlation function between (x, z) and $(x, z + l_0)$ is driven by the variance and outer scale at (x, z). A symmetric assessment is obtained through the redefinition

$$b_s(x, z_1, z_2, \vec{m}) = b_{vK}(\sigma_s^2(x, z_h, \vec{m}), l_s(x, z_h, \vec{m}), \Delta z), \tag{B5}$$

with $z_h = (z_1 + z_2)/2$ and $\Delta z = |z_2 - z_1|$. This is Eq. (13a).

The above relationships hold for temperature ($s = T$). After Wilson (1998, p. 1313), for incompressible, von Karman-type fluctuations, the longitudinal projected correlation function b_u of one velocity component writes as Eq. (13b). Wilson [1998, Eq. (76)] gives the relation between C_u^2, l_u and σ_u^2 [Eq. (14b)].

APPENDIX C: MOS RELATIONSHIPS

The MOS flux-profile relationships used in this study are given by

$$\langle u \rangle(z, u_*, F_T) = \frac{u_*}{k_{vK}} \left(\ln\left(\frac{z}{z_0}\right) - \Phi_m\left(\frac{z}{L}\right) + \Phi_m\left(\frac{z_0}{L}\right) \right), \tag{C1a}$$

$$\langle T \rangle(z, u_*, F_T) = T_{ref} + \frac{T_*}{k_{vK}} \left(\ln\left(\frac{z}{z_{ref}}\right) - \Phi_h\left(\frac{z}{L}\right) + \Phi_h\left(\frac{z_{ref}}{L}\right) \right) + \Gamma_d(z - z_{ref}), \tag{C1b}$$

where $T_* = -F_T/u_*$. The subscript *ref* refers to a reference value. The values $T_{ref} = 290\,\mathrm{K}$ at $z_{ref} = 10\,\mathrm{m}$ are used. The last term in the temperature profile relationship accounts for the impact of pressure relaxation on temperature; $\Gamma_d \approx -0.0098\,\mathrm{K\,m^{-1}}$ is the dry adiabatic lapse rate. The functions in Eq. (C1) follow from the formulas by Dyer (1974, see also Beljaars, 1994). The selected functions under unstable conditions are

$$\Phi_m(\varsigma) = 2\ln\left(\frac{1 + \phi_m^{-1}(\varsigma)}{2}\right) + \ln\left(\frac{1 + \phi_m^{-2}(\varsigma)}{2}\right) - 2\arctan\left(\phi_m^{-1}(\varsigma)\right) + \frac{\pi}{2}, \tag{C2a}$$

$$\Phi_h(\varsigma) = 2\ln\left(\frac{1+\phi_h^{-1}(\varsigma)}{2}\right), \quad \text{(C2b)}$$

$$\phi_m(\varsigma) = (1-16\varsigma)^{-1/4}, \quad \text{(C2c)}$$

$$\phi_h(\varsigma) = (1-16\varsigma)^{-1/2}. \quad \text{(C2d)}$$

The functions under stable conditions are given by

$$\Phi_m(\varsigma) = \Phi_h(\varsigma) = -5\varsigma. \quad \text{(C3)}$$

The wind variance is difficult to parameterize due to the wind isotropy assumption, which is never obeyed in experimental fits to MOS. Under unstable conditions, an empirical relationship is assumed in the form

$$\sigma_u^2(z, u_*, F_T) = u_*^2\left(\alpha_1 + \frac{1}{|L|}(\alpha_2 z_i + \alpha_3 z)\right)^{2/3}, \qquad L \le 0, \quad \text{(C4)}$$

where z_i is the boundary layer height, and the α's are numerical coefficients of the order of one. The dependence on the mixed layer height z_i accounts for the driving of the near-surface horizontal wind by the mixed layer dynamics under convective conditions. For simplicity, $z_i = 1000\,\mathrm{m}$ is set. The choice $\alpha_1 = 5.2$ and $\alpha_2 = 0.52$ matches the asymptotes of Wilson (2000) under neutral and convective conditions. The dependence on z accounts for the local free convection behavior of the vertical wind. One has $z \le 0.1 z_i$ in the surface layer, so this latter dependence is neglected ($\alpha_3 = 0$). Under stable conditions, the selected formulation inspires from Pahlow *et al*. (2001) and matches Eq. (C4) for $|L| \to \infty$:

$$\sigma_u^2(z, u_*, F_T) = u_*^2\left(1.73 + 3.3\left(\frac{z}{L}\right)^{0.5}\right)^2, \quad L > 0. \quad \text{(C5)}$$

The temperature variance is taken as

$$\sigma_T^2(z, u_*, F_T) = T_*^2 0.9\left(-\frac{z}{L}\right)^{-2/3}, \quad z/L \le -0.032, \quad \text{(C6a)}$$

$$\sigma_T^2(z, u_*, F_T) = 9T_*^2, \quad z/L > -0.032. \quad \text{(C6b)}$$

The first expression comes from Wyngaard *et al*. [1971, Eq. (28)]. The second comes from Pahlow *et al*. [2001, Eq. (15)], in which the dependence in z/L is ignored very near neutrality, whereby the expected cancelation of b_T through $\sigma_T^2 \approx 0$ and l_T finite.

The structure parameters C_T^2 and C_u^2 are parameterized as follows:

$$C_u^2(z, u_*, F_T) = \frac{u_*^2}{z^{2/3}} f_u\left(\frac{z}{L}\right), \quad \text{(C7a)}$$

$$C_T^2(z, u_*, F_T) = \frac{T_*^2}{z^{2/3}} f_T\left(\frac{z}{L}\right), \quad \text{(C7b)}$$

with (Edson and Fairall, 1998, Frederickson *et al*., 2000):

$$f_u(\varsigma) = 3.9\left(\frac{1-\varsigma}{1-7\varsigma} - \varsigma\right)^{2/3}, \quad \varsigma \le 0, \quad \text{(C8a)}$$

$$f_u(\varsigma) = 3.9(1+5\varsigma)^{2/3}, \quad \varsigma > 0, \quad \text{(C8b)}$$

$$f_T(\varsigma) = 5.9(1-8\varsigma)^{-2/3}, \quad \varsigma \le 0, \quad \text{(C8c)}$$

$$f_T(\varsigma) = 5.9\left(1+2.4\varsigma^{2/3}\right), \quad \varsigma > 0. \quad \text{(C8d)}$$

The relations for $f_u(\varsigma)$ stem from the relation $C_u^2 = 2.1\langle\varepsilon_e\rangle^{2/3}$, where ε_e is the dissipation rate of the turbulent kinetic energy. In near-neutral conditions, this parameterization is consistent with the shear-driven component of Wilson [2000, Eqs. (8) and (21)]. According to Eqs. (C7a) and (C8a), C_u^2 and $\langle\varepsilon_e\rangle$ depend only on the surface buoyancy flux under purely convective conditions. This asymptotic dependence is also obtained by Wilson [2000, Eqs. (9) and (21)]. The above relations yield $C_T^2 \approx 5.9T_*^2/z^{2/3}$ and $l_T \approx 1.9z$ near neutrality.

ANSI S12.18. (**1994**). *American National Standard Procedures for Outdoor Measurement of Sound Pressure Level* (Acoustical Society of America, New York).

Beljaars, A. C. (**1994**). "The parameterization of surface fluxes in large-scale models under free convection," Boundary Layer Meteorol. **121**, 255–270.

Cheinet, S. (**2003**). "A multiple mass-flux parameterization for the surface-generated convection. Part 1: Dry plumes," J. Atmos. Sci. **60**, 2313–2327.

Cheinet, S., (**2008**). "The variability of acoustical turbulence in the atmospheric boundary layer," in *Proceedings of the Acoustics'08 Conference (Paris)*, pp. 6, available at http://intellagence.eu.com/acoustics2008/acoustics2008/cd1/data/articles/001254.pdf (Last viewed October 12, 2011).

Cheinet, S., Beljaars, A. C., Köhler, M., Morcrette, J.-J., and Viterbo, P. (**2005**). "Validating physical processes in the ECMWF forecasts through the ARM SGP site measurements," ECMWF-ARM Technical Memorandum No. 1, pp. 25, available at www.ecmwf.int/publications/library/ecpublications/_pdf/ARM/ARM_RS1.pdf (Last viewed October 12, 2011).

Cheinet, S., Beljaars, A. C., Weiss-Wrana, K., and Hurtaud, Y. (**2011**). "The use of weather forecasts to characterise the near-surface optical turbulence," Boundary Layer Meteorol. **138**, 453–473.

Cheinet, S., and Cumin, P. (**2011**). "Local structure parameters of temperature and humidity in the entrainment-drying convective boundary layer: A LES analysis," J. Appl. Meteorol. **50**, 472–481.

Cheinet, S., and Naz, P. (**2006**). "On-going ISL research in modelling acoustic propagation in the atmosphere," NATO SET-107/RSY20/MSE Symposium, Amsterdam (Netherlands), pp. 11, available at www.dtic.mil/cgi-bin/GetTRDoc?Location=U2&doc=GetTRDoc.pdf&AD=ADA478770 (Last viewed October 12, 2011).

Cheinet, S., and Siebesma, A. P. (**2009**). "Variability of local structure parameters in the convective boundary layer," J. Atmos. Sci. **66**, 1002–1017.

Chevret, P., Blanc-Benon, P., and Juvé, D. (**1996**). "A numerical model for sound propagation through a turbulent atmosphere near the ground," J. Acoust. Soc. Am. **100**, 3587–3599.

Clifford, S. F., and Lataitis, R. L. (**1983**). "Turbulence effects on acoustic wave propagation over a smooth surface," J. Acoust. Soc. Am. **73**, 1545–1550.

Cotté, B., and Blanc-Benon, P. (**2007**). "Estimates of the relevant turbulent scales for acoustic propagation in an upward refracting atmosphere," Acta Acust. Acust. **93**, 1–15.

Daigle, G. A. (**1979**). "Effects of atmospheric turbulence on the interference of sound waves above a finite impedance boundary," J. Acoust. Soc. Am. **65**, 215–248.

Daigle, G. A., Embleton, T. F. V., and Piercy, J. E. (**1986**). "Propagation of sound in the presence of gradients and turbulence," J. Acoust. Soc. Am. **79**, 613–627.

Defrance, J., Salomons, E., Noordhoek, I., Heimann, D., Plovsing, D., Watts, G., Jonasson, H., Zhang, X., Premat, E., Schmich, I., Aballea, F.,

Baulac, M., and de Roo, F. (**2007**). "Outdoor sound propagation reference model developed in the European Harmonoise project," Acta Acust. Acust. **93**, 213–227.
Dyer, A. J. (**1974**). "A review of flux-profile relationships," Boundary Layer Meterol. **7**, 363–372.
Edson, J. B., and Fairall, C. W. (**1998**). "Similarity relationships in the marine atmospheric surface layer for terms in the TKE and scalar variance budgets," J. Atmos. Sci. **55**, 2311–2328.
Forssén, J. (**2003**). "An extended substitute-sources method for a turbulent atmosphere: calculation for upward refraction," Acta Acust. Acust. **89**, 225–233.
Frederickson, P. A., Davidson, K. L., Zeisse, C. R., and Bendal, C. S. (**2000**). "Estimating the refractive index structure parameter (C_n^2) over the ocean using bulk methods," J. Appl. Meteorol. **39**, 1770–1789.
Gilbert, K. E., Raspet, R., and Di, X. (**1990**). "Calculation of turbulence effects in an upward-refracting atmosphere," J. Acoust. Soc. Am. **87**, 2428–2437.
Gilbert, K., and White, M. (**1989**). "Application of the parabolic equation to sound propagation in a refracting atmosphere," J. Acoust. Soc. Am. **85**, 630–637.
Havelock, D. I., Di, X., Daigle, G. A., and Stinson, M. R. (**1995**). "Spatial coherence of a sound field in a refractive shadow: Comparison of simulation and experiment," J. Acoust. Soc. Am. **98**, 2289–2302.
Heimann, D., and Gross, G. (**1999**). "Coupled simulation of meteorological parameters and sound level in a narrow valley," Appl. Acoust. **56**, 73–100.
Heimann, D., and Salomons, E. M. (**2004**). "Testing meteorological classifications for the prediction of long-term average sound levels," Appl. Acoust. **65**, 925–950.
Lihoreau, B., Gauvreau, B., Bérengier, M., Blanc-Benon, P., and Calmet, I. (**2006**). "Outdoor sound propagation modeling in realistic environments: Application of coupled parabolic and atmospheric models," J. Acoust. Soc. Am. **120**, 110–119.
Macaskill, C., and Ewart, T. E. (**1984**). "Computer simulation of two-dimensional random wave propagation," J. Appl. Math. **33**, 1–15.
Ostashev, V. E. (**1994**). "Sound propagation and scattering in media with random inhomogeneities of sound speed, density and medium velocity," Waves Rand. Med. **4**, 403–418.
Ostashev, V. E. (**1997**). *Acoustics in Moving Inhomogeneous Media* (E&F Spon, London), Chap. 2 and 7.
Ostashev, V. E., Juvé, D., and Blanc-Benon, P. (**1997**). "Derivation of a wide-angle parabolic equation for sound waves in inhomogeneous moving media," Acta Acust. Acust. **83**, 455–460.
Ostashev, V. E., and Wilson, D. K. (**2000**). "Relative contributions from temperature and wind velocity fluctuations to the statistical moments of a sound field in a turbulent atmosphere," Acta Acust. Acust. **86**, 260–268.
Pahlow, M., Parlange, M. B., and Porté-Agel, F. (**2001**). "On Monin-Obukhov similarity in the stable atmospheric boundary layer," Boundary Layer Meterol. **99**, 225–248.
Parkin, P. H., and Scholes, W. E. (**1964**). "The horizontal propagation of sound from a jet engine close to the ground, at Radlett," J. Sound Vib. **1**, 1–13.
Parkin, P. H., and Scholes, W. E. (**1965**). "The horizontal propagation of sound from a jet engine close to the ground, at Hatfield," J. Sound Vib. **2**, 353–374.
Salomons, E. M. (**1998**). "Improved Green's function parabolic equation method for atmospheric sound propagation," J. Acoust. Soc. Am. **98**, 100–111.
Salomons, E. M., and Heimann, D. (**2004**). "Description of the Reference model," Technical Report of the HARMONOISE project, pp. 33.
Salomons, E., van Maercke, D., Defrance, J., and de Roo, F. (**2011**). "The Harmonoise sound propagation model," Acta Acust. Acust. **97**, 62–74.
Tatarski, V. I. (**1961**). *Wave Propagation in a Turbulent Medium* (McGraw-Hill, New York), Chap. 7.
van Maercke, D., and Defrance, J. (**2007**). "Development of an analytical model for outdoor sound propagation within the Harmonoise project," Acta Acust. Acust. **93**, 201–212.
Wasier, J. (**1999**). "Etude expérimentale des effets d'une frontière sur la propagation des ondes acoustiques à travers une turbulence thermique (Experimental study of the effects of a boundary on the sound propagation through thermal turbulence)," Ph.D. thesis, Ecole Centrale de Lyon, Lyon, France, pp. 183.
West, M., Gilbert, K., and Sack, R. A. (**1992**). "A tutorial on the Parabolic Equation (PE) model used for long range sound propagation in the atmosphere," Appl. Acoust. **37**, 31–49.
West, M., Walkden, F., and Sack, R. A. (**1989**). "The acoustic shadow produced by wind speed and temperature gradients close to the ground," Appl. Acoust. **27**, 239–260.
Wiener, F. M., and Keast, D. N. (**1959**). "Experimental study of the propagation of sound over ground," J. Acoust. Soc. Am. **31**, 724–733.
Wilson, D. K. (**1998**). "Performance bounds for the acoustic direction-of-arrival arrays operating in atmospheric turbulence," J. Acoust. Soc. Am. **103**, 1306–1319.
Wilson, D. K. (**2000**). "A turbulence spectral model for sound propagation in the atmosphere that incorporates shear and buoyancy forcings," J. Acoust. Soc. Am. **108**, 2021–2038.
Wilson, D. K. (**2003**). "The sound-speed gradient and refraction in the near-ground atmosphere," J. Acoust. Soc. Am. **113**, 750–757.
Wilson, D. K., and Ostashev, V. E. (**2001**). "Statistical moments of the sound field propagating in a random, refractive medium near an impedance ground," J. Acoust. Soc. Am. **109**, 1909–1921.
Wilson, D. K., Ostashev, V. E., and Lewis, M. S. (**2009**). "Moment-screen method for wave propagation in a refractive medium with random scattering," Waves Rand. Med. **19**, 369–391.
Wunderli, J. M., and Rotach, M. W. (**2011**). "Application of statistical weather data from the numerical weather prediction model COSMO-2 for noise mapping purposes," Acta Acust. Acust. **97**, 403–415.
Wyngaard, J. C., Cotté, O. R., and Izumi, Y. (**1971**). "Local free convection, similarity, and the budgets of shear stress and heat flux," J. Atmos. Sci. **28**, 1171–1182.